

Polarized cathodoluminescence study of selectively grown self-assembled InAs/GaAs quantum dots

D. H. Rich,^{a)} Y. Tang, A. Konkar, P. Chen, and A. Madhukar
*Photonic Materials and Devices Laboratory, Department of Materials Science & Engineering,
University of Southern California, Los Angeles, California 90089-0241*

(Received 8 June 1998; accepted for publication 2 September 1998)

We have examined the optical properties of self-assembled InAs quantum dots (QDs) grown on prepatterned GaAs(001) substrates with polarization sensitive and time-resolved cathodoluminescence (CL) imaging and spectroscopy techniques. The InAs QDs were formed using a novel application in self-assembled molecular beam epitaxial growth, which entailed the growth of InAs on preformed $[1\bar{1}0]$ -oriented stripe mesas. Interfacial In adatom migration occurred along the stripe side-walls during growth, enabling the selective formation of linear arrays of InAs QDs on the stripe mesas. The total InAs deposition needed to induce the two-dimensional to three-dimensional morphology change on the stripes is less than that required to initiate QD formation on the unpatterned substrates. The QDs formed on the mesa top were found with a luminescence distribution redshifted relative to QDs in the valley region, indicating that QDs with a larger average size were formed on the mesa top. The lower density of QDs in the valley region led to a weaker emission and sharper δ -like transitions at lower beam currents, relative to emission from QDs on the mesa. CL imaging was employed to study the spatial distribution of luminescence and identified the presence of relatively small QDs situated near the edges of the valley region along the lower surface of the stripe edges. An excitation- and energy-dependent polarization anisotropy relative to the $\langle 110 \rangle$ directions was observed in CL emission. A polarization anisotropy reversal was found between CL from QDs on the mesa and in the valley regions, revealing the importance of the stress anisotropy in both the formation of QDs and their subsequent optical properties. The CL was examined as a function of temperature to evaluate the thermal re-emission of carriers and the associated activation energies. The carrier relaxation kinetics were studied with time-resolved CL to measure differences in the CL onset and decay rates for QDs in the valley and mesa regions.
© 1998 American Institute of Physics. [S0021-8979(98)05323-7]

I. INTRODUCTION

The molecular beam epitaxial (MBE) growth of InAs self-assembled quantum dots (SAQDs) on GaAs has in recent years drawn a great deal of attention, owing to its great potential for applications in lasers,^{1,2} infrared detectors,^{3,4} and single-electron transistors.^{5,6} The MBE growth and formation of a high density of strained pyramidal InAs islands on unpatterned GaAs(001) substrates has been demonstrated and systematically studied by a number of authors.⁷⁻¹⁰ The density and size distribution of the InAs QDs as a function of InAs coverage has been studied in detail using scanning tunneling microscopy (STM) and atomic force microscopy (AFM).¹¹⁻¹³ The InAs SAQDs form with a substantial variation in size, thereby yielding a unique spectrum of confined δ -like states for each QD. The inhomogeneity in height and lateral size of the SAQDs results in a broad (40–60 meV) luminescence line shape, whose width depends on the level of excitation.¹⁰

Various attempts have been made to control the size, shape, and spatial arrangement of InAs SAQDs.¹¹⁻¹⁵ Experiments have shown that SAQDs, at the later stages of growth, have a tendency toward lateral size equalization, owing to a

strain-dependent incorporation and elastic interaction of islands through the substrate.¹¹⁻¹³ Vertical self-organization of the islands has been demonstrated by utilizing the strain field in the cap layers induced by three-dimensional (3D) islands as a driving force.^{11,14} Recently, a lateral spatial selectivity in the control of InAs SAQD formation has been demonstrated by the growth of InAs on patterned GaAs(001) substrates.¹⁵ Owing to a stress-driven interfacial In adatom migration on GaAs mesa sidewalls, parallel chains of InAs SAQDs on GaAs stripe mesa tops have been fabricated.¹⁵ Optoelectronic devices based on SAQD active regions will likely benefit from innovations in the stress engineering employed to control the size and shape uniformity, lateral arrangement, and ordering of QDs. Thus, it is necessary to explore the extent to which the patterning geometry, cation migration, and residual strain fields during the SAQD formation will impact its subsequent optical properties.

Temperature- and excitation-dependent photoluminescence (PL),¹⁶⁻¹⁸ polarized PL,^{19,20} and time-resolved PL studies²¹⁻²³ have been performed by several authors for InAs SAQDs grown on unpatterned GaAs substrates. In this paper, we report on the optical properties of InAs QDs grown selectively on top of mesa stripes prepatterned into GaAs(001) substrates. The studies were carried out utilizing polarization sensitive, excitation- and temperature-

^{a)}Electronic mail: danrich@almaak.usc.edu

dependent, and time-resolved cathodoluminescence (CL) imaging and spectroscopy techniques. In order to achieve the desired GaAs substrate template for spatially selective growth of linear arrays of SAQDs, we employed a size reducing epitaxial growth to obtain, *in situ*, mesa top widths of less than ~ 200 nm.^{15,24} Subsequently, In adatom interfacet migration occurred during the InAs growth on stripe side walls that possessed a prearranged facet orientation and enabled the selective formation of InAs QDs on stripe mesas.¹⁵ The total InAs deposition needed to induce the 2D to 3D morphology change on the stripes is less than that required to initiate QD formation on the unpatterned substrates, owing to the In migration on the mesa side walls.¹⁵ An energy- and excitation-dependent polarization anisotropy was observed in CL emission from QDs. A reversal in the primary linear polarization orientation is found between QDs residing on and off the mesas, revealing the importance of the stress anisotropy in both the formation of QDs and their subsequent optical properties.

II. SAMPLES AND EXPERIMENTAL SETUP

InAs SAQD structures were grown by MBE on prepatterned GaAs(001) substrates. The details of the sample preparation and growth have been described elsewhere.^{11,15} A GaAs(001) substrate patterned with stripes along the $[\bar{1}\bar{1}0]$ direction was prepared by chemical etching and followed by an *in situ* size reducing GaAs epitaxial growth to achieve the desired shapes of the sidewall facets prior to the deposition of InAs. The control of the size, shape, and orientation of the $\{114\}/\{113\}$ type sidewall facets is essential in creating a migration path that allows In mass transport along the mesa sidewalls during growth.^{15,24} The current GaAs etching and regrowth procedure enabled a trapezoidal mesa shape, elongated along the $[\bar{1}\bar{1}0]$ direction, to have upper and lower base widths of ~ 0.2 and ~ 2 μm , respectively. The distance between the centers of neighboring stripes is ~ 4 μm . Subsequent to the GaAs mesa preparation, 1.45 monolayer (ML) of InAs was deposited at 500°C . A separate AFM study of samples grown in this way for mesa top widths less than 0.2 μm showed that SAQDs form on the mesa top for an InAs delivery of 1.45 ML owing to In migration from the sidewalls to the mesa top. When the upper width of the stripe mesas exceeds ~ 0.2 μm , SAQDs do not form for the same InAs delivery of 1.45 ML,¹⁵ thereby indicating a critical interplay between InAs delivery, mesa geometry, and SAQD formation. AFM measurements showed that the average InAs island density on ~ 0.1 μm wide mesa tops is ~ 1000 μm^{-2} , resulting in an average island spacing of ~ 30 nm. AFM also showed the presence of parallel rows of QDs on the mesa tops. The SAQDs were capped with a 50 nm thick GaAs layer grown by migration enhanced epitaxy. The unpatterned planar region, far from the patterned part of the sample, is expected to exhibit no QD formation since the 1.45 ML InAs delivery is less than that required to initiate QD formation on a planar GaAs(001) substrate.¹¹⁻¹³

The CL experiments were performed with a modified JEOL-840A scanning electron microscope (SEM) using a 15 keV electron beam with probe current ranging from 0.1 to 10

nA. The temperature (T) of the sample was varied from 87 to 200 K. Details of the optical collection system have been previously reported.²⁵ CL spectra were obtained with a 0.275 m monochromator and a Si charge coupled device (CCD) detector, enabling a maximum spectral resolution of 0.1 nm. For monochromatic CL imaging and time-resolved CL experiments, a Si avalanche photodiode was used. The method of delayed coincidence in an inverted single photon counting mode was employed for the time-resolved study with a time resolution of ~ 100 ps.²⁵ Electron beam pulses of 50 ns width with a 1 MHz frequency were used to excite the sample. Linearly polarized cathodoluminescence (LPCL) measurements were performed by detecting luminescence with a rotatable vacuum linear polarizer mounted in the SEM chamber.²⁶ Luminescence was detected with the electric field (\mathbf{E}) along either the $[110]$ or $[\bar{1}\bar{1}0]$ directions to evaluate the presence of an anisotropy caused by strain or quantum confinement.

III. RESULTS AND DISCUSSION

A. Spectrally and spatially resolved CL of the mesa and valley regions

SEM and corresponding CL plan view monochromatic images of the sample maintained at $T=87$ K are shown in Fig. 1(a). The various wavelengths shown were chosen after a series of local CL spectra were acquired by fixing the e beam on a spot during the spectral acquisition. A beam current I_b of 1 nA was used. The arrows in the images are used as a marker to reference the same position on the sample for all images. The tips of the arrows point to the approximate center position ($\Delta x=0$) of a mesa stripe. The white vertical line in the SEM image delineates a line along which the e beam was positioned. Figure 1(b) illustrates the positioning of the electron beam along a line with variable distance, Δx , relative to center of a mesa top so as to acquire CL spectra with a localized excitation. Such local CL spectra were obtained to assess the spatial variation in the SAQD emission, as shown in Fig. 2. A spatial variation in the spectra is expected, owing to a facet-dependent In cation migration that can occur on a length scale of ~ 1 μm during MBE growth leading to a spatially dependent SAQD density.^{14,27} The CL spectra exhibit a broad (~ 50 nm) asymmetric hump centered at ~ 950 nm when the e beam is positioned near the center of a stripe mesa ($\Delta x=0$). The spectra gradually exhibit a sharper multicomponent line shape with the center of gravity blueshifted by ~ 30 nm as the e beam is positioned near the center of the region between the stripes (i.e., the valley region) at $\Delta x=1.91$ μm . Given the mesa shape and bottom width, this corresponds to a separation of less than 1 μm from the bottom edge of the mesa. The distinct emission at 868 nm in the valley region is due to the excitonic recombination in the InAs wetting layer (WL).⁸ This emission is noticeably absent for excitation on the mesa top ($\Delta x=0$), revealing marked differences in the carrier relaxation and collection in the QDs between the mesa top and valley regions.

The broad emission peaks with wavelengths greater than ~ 880 nm are due to excitonic recombination in QDs for the

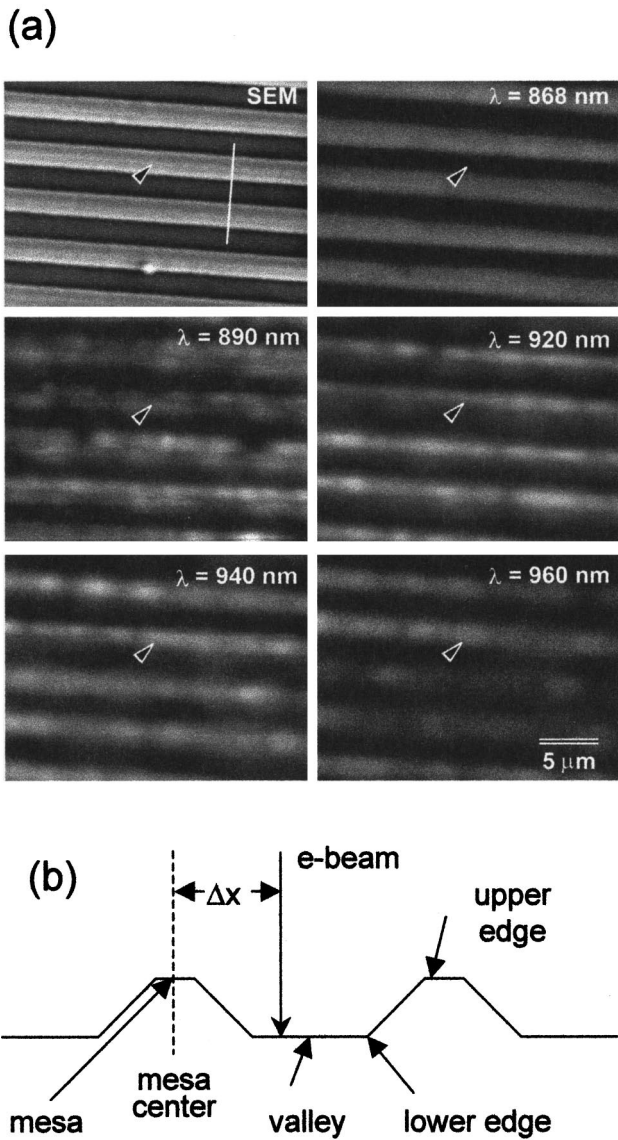


FIG. 1. SEM and CL images of the InAs QD sample showing the valley and mesa regions (a) and a schematic diagram showing a cross-sectional view of the mesas and positioning of the e beam with variable distance Δx relative to the center of a mesa top (b). The arrows in (a) point to the same location on a mesa stripe for all images. Monochromatic CL images are shown for various wavelengths, as indicated.

e beam positioned in both the mesa top and valley regions. The presence of QD emission for an e beam positioned in the mesa top regions is expected, given the AFM results on the existence of SAQDs on mesa tops.¹⁵ The presence of such an emission for excitation in the valley region, less than $1 \mu\text{m}$ from the mesa bottom edges, indicates that In migration along the facet sidewalls occurred towards the valley region as well, and some SAQDs formed near the valley edges. The In deposition of 1.45 ML is less than the ~ 1.57 ML coverage required to initiate QD formation on an unpatterned GaAs sample.¹¹⁻¹³ CL spectra of an unpatterned region of this sample, far from the stripe mesas, confirms the absence of a QD luminescence and the presence of only the WL emission. Thus, these CL results show that the In migration yields an effective local coverage greater than ~ 1.57 ML on the mesa tops as well as the mesa bottom edges (i.e., the

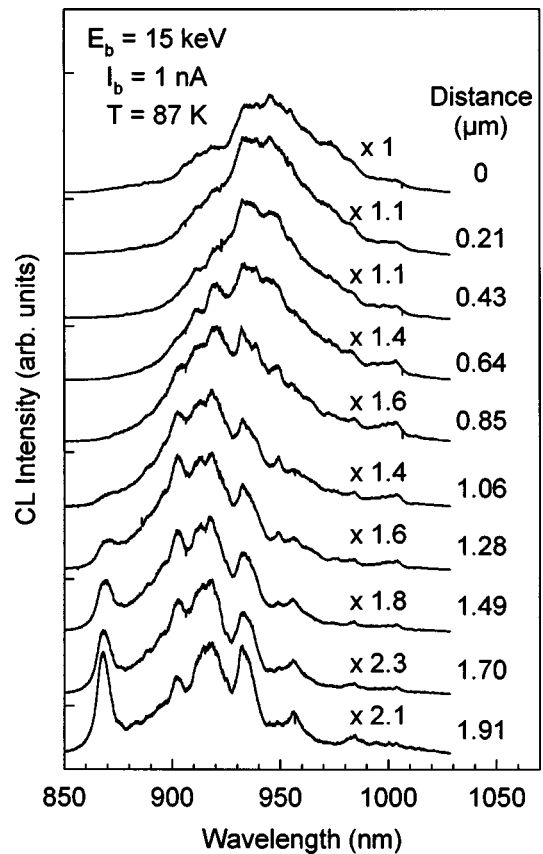


FIG. 2. Local CL spectra acquired along a line orthogonal to the mesa stripes (i.e., along the white line in the SEM image of Fig. 1) for various distances relative to the center of a mesa. The distance of 0 refers to the center of a mesa stripe and a distance of $1.91 \mu\text{m}$ is close to the center of a valley region.

valley edges), thereby yielding QDs in both regions. The ~ 30 nm blueshift of the center of gravity of the QD luminescence in the valley edge region relative to the mesa top indicates that the QDs in the valley possess a distribution of smaller or more strained QDs relative to the ensemble residing on the mesa tops. The reduced total SAQD emission when the beam is positioned in the valley region indicates a reduced average density of QDs in the valley relative to the mesa tops. We note that the center wavelength positions of the CL spectra for excitation of both the mesa top and valley regions are blueshifted by 50–100 nm relative to that for samples with SAQDs grown on planar substrates under similar growth conditions.^{10,11,16-23} Thus, the stress-driven cation migration is evidently responsible for creating an ensemble of smaller QDs or QDs possessing larger average compressive strains relative to SAQDs grown on planar substrates.

A line scan analysis of the CL imaging data is shown in Fig. 3 showing a plot of the CL intensity versus the position along a direction perpendicular to the stripes. The zero point baseline is shown for each line scan to illustrate the difference in relative intensity between QD emission on the mesa and valley edge regions. A distinct broadening and double peak behavior in the 890 nm CL image and 890 nm line scan is observed in Figs. 1 and 3. These intensity peaks are separated by $\sim 1.1 \mu\text{m}$. The full width at half maximum (FWHM) of the 890 nm peak in the line scan is $\sim 2.2 \mu\text{m}$.

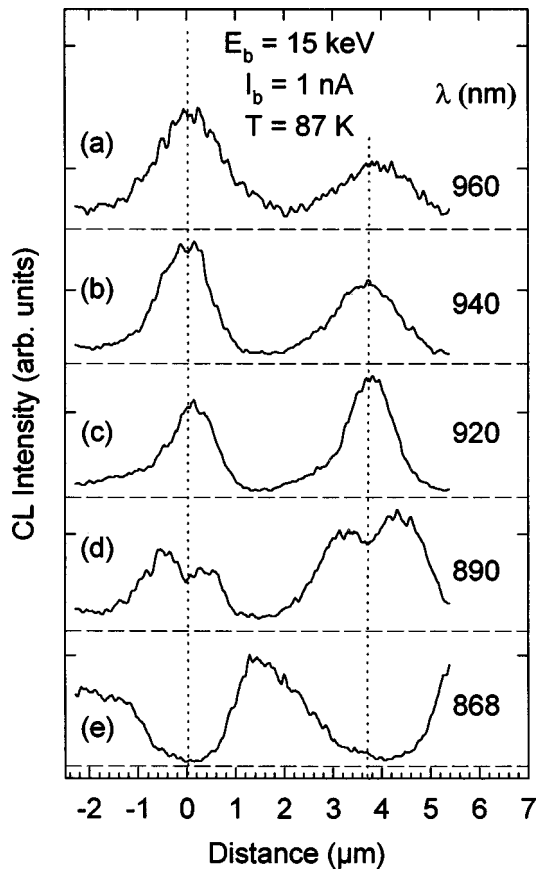


FIG. 3. A monochromatic line scan analysis of the CL images shown in Fig. 1.

Thus, this spatial distribution also suggests that the 890 nm emission arises from a group of relatively small QDs situated near the edges of the valley region along the lower surface of the stripe edges.

B. Excitation and polarization dependent CL

The spectral line shape of the QD luminescence depends sensitively on the excitation conditions. Strong band filling effects have been observed in CL and PL studies of InAs SAQDs grown on unpatterned GaAs(001) substrates.^{10,16} These studies have revealed a net blueshift in the QD emission caused by the filling of the ground states in the QDs and subsequent excitonic transitions involving the higher lying hole states.¹⁶ In the present study, the QDs were probed with various beam currents from 0.1 to 10 nA by positioning the electron beam on the center of the mesa top and in the center of the valley region, as shown in Figs. 4 and 5, respectively. A polarization sensitive detection was employed, and emission was detected with $\mathbf{E} \parallel [1\bar{1}0]$ or $\mathbf{E} \perp [1\bar{1}0]$, as shown in Figs. 4 and 5. For both QD emission on the mesa and in the valley edge regions, the CL spectra are observed to broaden and blueshift as the beam current is increased from 0.1 to 10 nA. The sharp and dispersed peaks observed in the CL spectra acquired in the valley region for $0.1 \leq I_b \leq 0.5$ nA are indicative of the discrete δ -like nature of the QD density of states, as previously observed in CL and PL studies of QDs grown on unpatterned substrates.⁸⁻¹⁰ Although the line shape

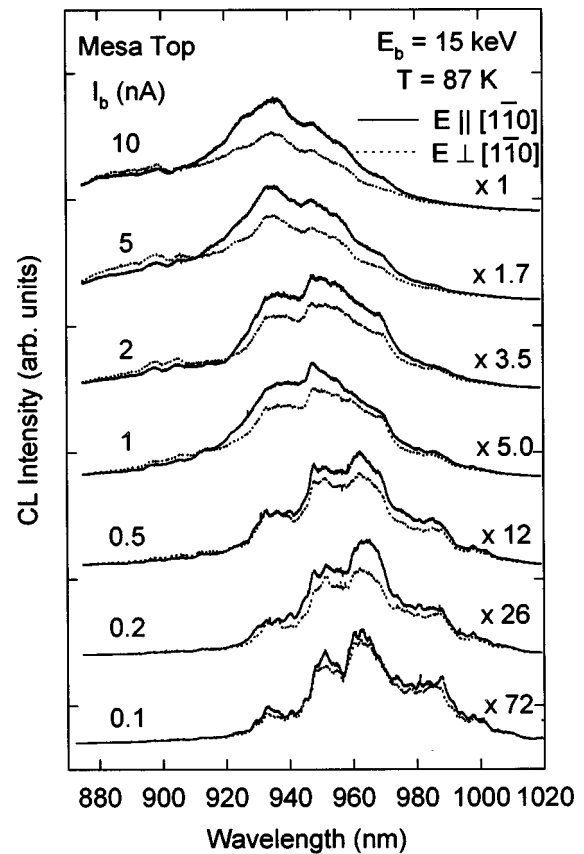


FIG. 4. Linear polarized CL spectra of the mesa top for various electron beam currents. CL was detected with the electric field \mathbf{E} oriented with $\mathbf{E} \parallel [1\bar{1}0]$ (solid lines) or $\mathbf{E} \perp [1\bar{1}0]$ (dashed lines).

of the QD emission on the mesa top narrows for $I_b \leq 0.5$ nA, the linewidth of each peak is noticeably broader than that observed for excitation of the valley region. The more discrete nature of the QD luminescence in the valley edge region reflects a significantly reduced magnitude of the QD density relative to the mesa top. The excitation and diffusion volume of the e-beam probe will enable a sampling of $\sim 1 \mu\text{m}^2$ of the surface area, resulting in an excitation on the order of ~ 100 QDs in the mesa top regions. The significantly lower average density of QDs in the valley region would enable the more discrete nature of the QDs to be observed, particularly for the lowest beam currents, as shown in Fig. 5. The number of discrete peaks observed in the valley edge region, together with an estimated lateral carrier diffusion length of $\sim 0.5 \mu\text{m}$, suggests an average QD density on the order of $10 \mu\text{m}^{-2}$ in the valley edge region, which is two orders of magnitude lower than the QD density on the mesa top.

An excitation-dependent polarization anisotropy is observed in Figs. 4 and 5 for QD emission from the mesa top and valley edge regions, respectively. A striking feature of the data is the reversal in the polarization anisotropy between the mesa top and valley edge regions. The integrated polarized CL intensity ratio for QD emission, $I_{[1\bar{1}0]}/I_{[110]}$, versus beam current is shown in the upper panel of Fig. 6. The lower panel of the figure shows the integrated CL intensities of the QD emission, WL emission, and GaAs substrate emis-

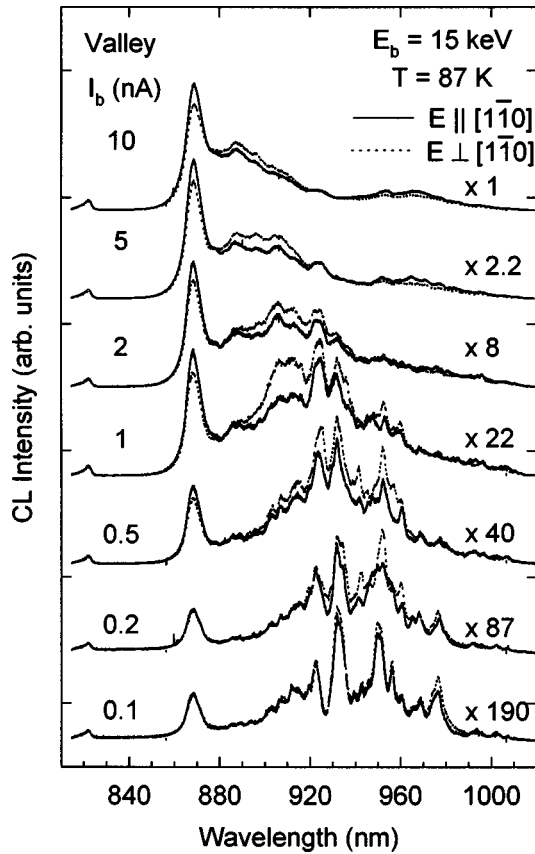


FIG. 5. Linear polarized CL spectra of the valley region for various electron beam currents. CL was detected with the electric field E oriented with $E \parallel [110]$ (solid lines) or $E \perp [110]$ (dashed lines).

sions in both the valley and mesa top regions versus the beam current. The WL emission is observed to increase at a faster rate than the QD emission in the valley region as I_b is increased from 1 to 10 nA. As state filling of the QDs occurs for higher beam currents, the rate of transfer of carriers from the WL is expected to be reduced and thus leads to a proportionally larger emission from the WL. $I_{[1\bar{1}0]}/I_{[110]}$ for QDs on the mesa top is observed to monotonically increase from ~ 1.1 to 1.2 as the beam current is increased from 0.1 to 10 nA. A nonmonotonic dependence in the polarization ratio versus I_b is observed for the valley region as $I_{[1\bar{1}0]}/I_{[110]}$ decreases from 0.93 to 0.81 as I_b is increased from 0.1 to 0.5 nA and then increases back to 0.93 as I_b is further increased to 10 nA.

Previously, linearly polarized cathodoluminescence measurements have been employed to study the influence of strain on the optical properties of strained $(\text{InP})_2/(\text{GaP})_2$ quantum wires.²⁸ The presence of a strain can effect the relative admixtures of heavy-hole (hh) and light-hole (lh) characters in the valence-band wave functions, thereby inducing polarization effects in the excitonic luminescence.^{26,28} Such measurements can be employed to help distinguish between states possessing varying degrees of hh and lh admixtures, provided that the form of the strain tensor and geometry of the nanostructure are well understood. For the present data, the reversal in the polarization anisotropy between QD emission in the valley edge and mesa top regions can be attrib-

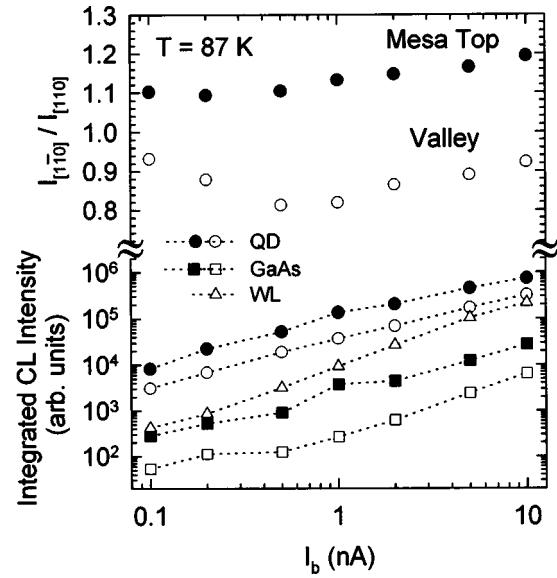


FIG. 6. The integrated polarization intensity ratio, $I_{[1\bar{1}0]}/I_{[110]}$, vs beam current for the QD emission (upper panel) and integrated CL intensity vs beam current for the QD, WL, and GaAs near-band-edge emissions (lower panel). Filled symbols and open symbols denote the mesa top and valley regions, respectively.

uted to differences in the strain experienced by QDs situated in the valley edge and mesa top regions, owing to differences in the interfacet cation migration rates, effective InAs coverage, the QD size and shape distribution, and the local QD density, all of which can influence the resulting strain fields experienced by the QDs. The excitation dependence of $I_{[1\bar{1}0]}/I_{[110]}$, concomitant with the state filling effects observed in the QD CL line shape, suggest that the various higher lying hole states, possessing varying admixtures of hh and lh characters, are filled and participate in the excitonic luminescence as the beam current is increased over the 0.1–10 nA range. The broadening of the CL line shape and shift in the center of gravity towards shorter wavelengths in both regions (Figs. 4 and 5) are consistent with these state filling effects. Moreover, the polarization ratio is observed to be wavelength dependent for QD emission in the valley edge region (Fig. 5) for $I_b \geq 2$ nA. $I_{[1\bar{1}0]}/I_{[110]}$ is observed to be less than one for $880 \leq \lambda \leq 920$ nm and is greater than one for $940 \leq \lambda \leq 1000$ nm in the valley region. We therefore consider the possibility that size and shape fluctuations of the QDs in the valley edge region will lead to variations in strain and in the mixing of hh and lh characters in the excited QD states.

C. Temperature dependence of the QD emissions in the mesa and valley edge regions

We have explored the temperature dependence of the QD emission in an intermediate temperature (T) range between 87 and 200 K. Local CL spectra are shown for various temperatures for the QD emission on the mesa top and in the valley edge regions in Figs. 7 and 8, respectively. Certain luminescence features in the QD emission are actually observed to sharpen slightly as the temperature is increased over the $106 \leq T \leq 135$ K and $106 \leq T \leq 165$ K ranges for the

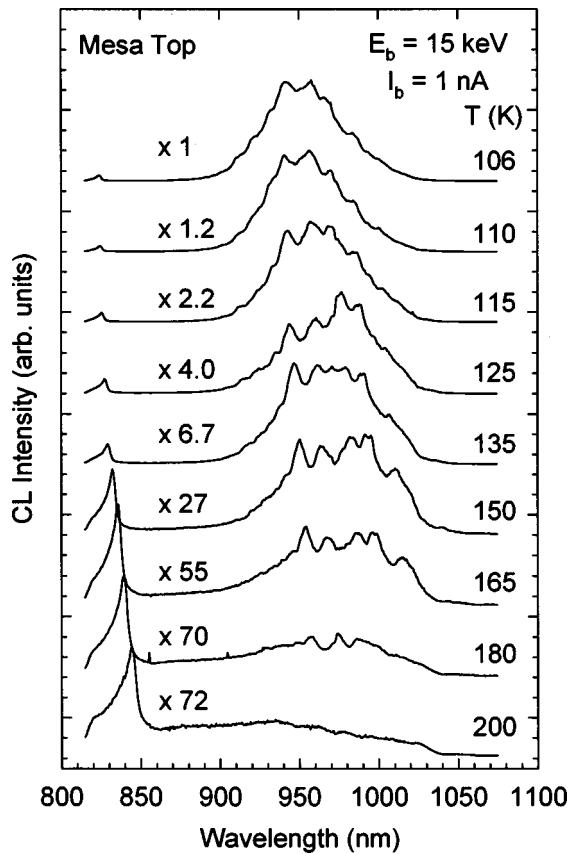


FIG. 7. Local CL spectra of the mesa top for the various temperatures indicated.

valley edge and mesa top regions, respectively. The discrete peaks in the spectra can be traced from one spectra to another as the temperature is increased over these ranges. The added discreteness at higher temperatures may reflect the thermal excitation of holes into closely spaced higher lying states, thereby giving the spectral line shape more structure for higher temperatures. The QD, WL, and GaAs band-edge features are all observed to redshift as the temperature is increased in accordance with the usual temperature dependence of the band gap, as predicted by the Varshni relation.²⁹

The integrated CL intensities of the QD, WL, and GaAs band-edge luminescence are shown for various temperatures in Fig. 9, the closed and open symbols representing the mesa top and valley edge regions, respectively. The data are shown in a log of CL intensity versus $1/kT$ plot. An Arrhenius behavior for the CL intensities is observed, and a linear fit to the data yields activation energies of 123 and 80 meV, respectively, for the QD and WL emissions in the valley edge region. The decrease in the QD emission with increasing temperature is evidently due to the increase in thermal re-emission of captured excitons. Electrons and holes in the QDs can be re-emitted to the WL or GaAs barrier prior to their radiative recombination in the QDs, provided that the thermal energy permits a sufficiently large rate of re-emission. The carriers can then recombine through other radiative and nonradiative channels in the WL or GaAs barrier. The 123 meV activation energy is very close to the energy difference between the WL emission ($\lambda \approx 868$ nm at 87 K)

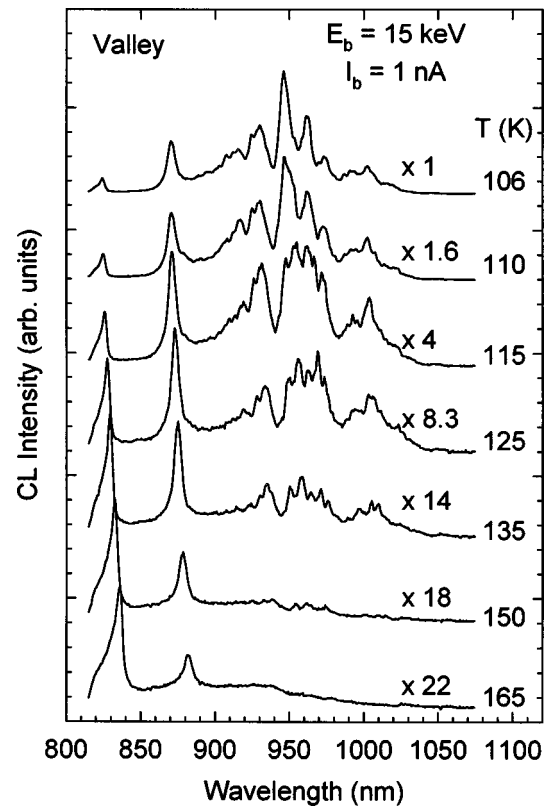


FIG. 8. Local CL spectra of the valley region for the various temperatures indicated.

and the center of the QD spectral emission ($\lambda \approx 930$ nm) in the valley region, thus providing strong evidence that thermal re-emission of carriers from the QDs to the WL occurs in the $105 \leq T \leq 200$ K temperature range. The Arrhenius be-

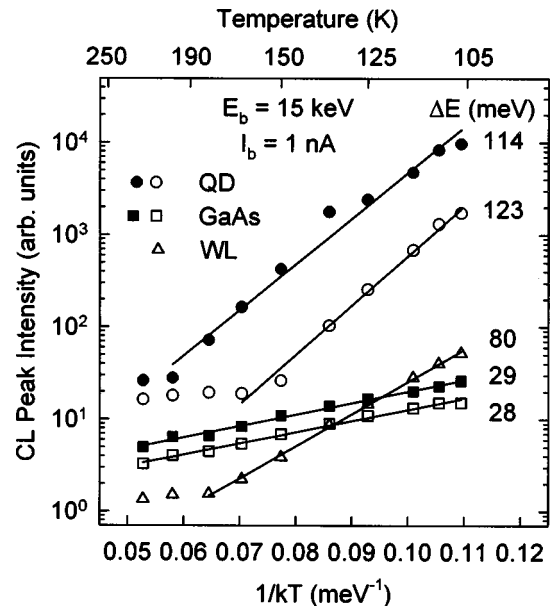


FIG. 9. The integrated CL intensity of the QD, WL and GaAs near-band-edge emissions vs $1/kT$. Filled symbols and open symbols denote the mesa top and valley regions, respectively. Solid lines indicate the results of linear fits in a temperature range which exhibits an Arrhenius behavior. Activation energies were obtained from the slopes of the fits and are indicated.

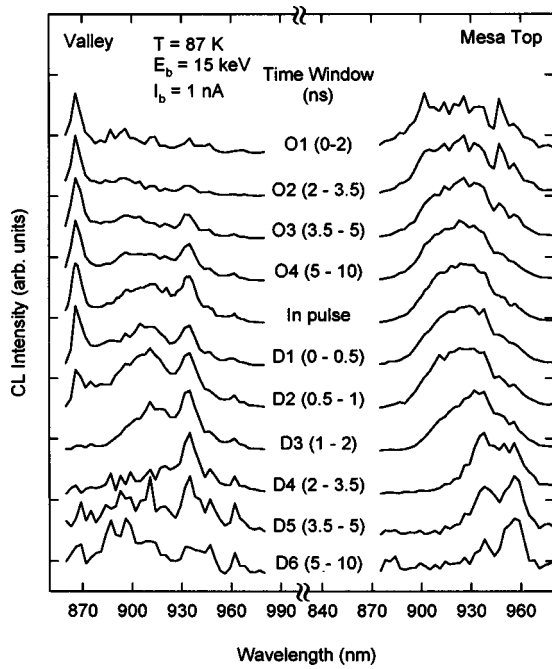


FIG. 10. Time delayed CL spectra for the (a) mesa top and (b) valley region. The spectra are shown for various onset (O_i) and decay (D_i) time windows. All spectra are renormalized to have about the same maximum peak height.

havior of the WL emission is also an indication that carriers will be thermally re-emitted into the GaAs matrix. Again, the energy difference of the GaAs band-edge ($\lambda \approx 823$ nm) and WL emissions, which is ~ 78 meV, confirms this behavior.

The activation energy for re-emission from the QDs on the mesa top is 114 meV and is very close to that obtained for QD emission in the valley edge region. The value of this activation energy is strong evidence for the existence of a WL on the mesa top, in spite of its lack of optical activity (i.e., absence of luminescence). The energy difference between the center of the QD spectral emission on the mesa top ($\lambda \approx 950$ nm at 87 K) and the GaAs band-edge emission ($\lambda \approx 823$ nm) is ~ 200 meV, which is nearly double the measured activation energy. Thus, the energetics appear to support the existence of a WL. We can only suggest that the high density of QDs on the mesa top and fast relaxation from the WL to the QDs or existence of nonradiative recombination may suppress radiative recombination of carriers in the WL on the mesa top.

D. Time-resolved CL measurements

The carrier relaxation kinetics have been studied with time-resolved CL measurements. A series of CL transients were taken with the wavelength ranging from 880 to 980 nm at a temperature of 87 K. Time delayed spectra of the mesa top and valley emissions were reconstructed from the CL transients, as shown in Fig. 10. The spectrum labeled *in pulse* was acquired with the time window centered in the middle of the 50 ns excitation pulse, thereby obtaining spectra similar to the constant excitation CL measurements. Spectra are shown for various time windows during the onset and decay phases, denoted as O_i and D_i . During the earliest

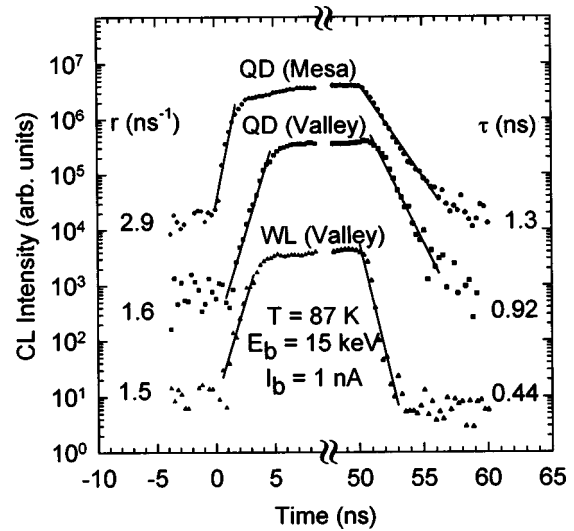


FIG. 11. The integrated CL intensity vs time for emissions from the QDs on the mesa, QDs in the valley, and the WL in the valley shown in a semilogarithmic plot. Linear fits (solid lines) were performed to determine the onset rates r and decay times τ .

onset window, O_1 , which is centered at 1 ns after the rising edge of the excitation pulse, relatively sharp and distinct features are observed in the QD emission in the 880–980 nm wavelength range. These features gradually broaden and lose structure as the windows progress from O_2 to O_4 (Fig. 10). This broadening is evidently due to time-dependent state filling effects that occur during the carrier relaxation and collection into QDs. The system eventually proceeds towards the steady state, as reflected by the spectra labeled *in pulse*. The WL emission, in spectra for the valley region, show a strong emission throughout all onset windows in Fig. 10, indicating a rapid carrier collection by the WL.

During the decay, a rapid redshift and narrowing is seen to occur, indicating that carriers are relaxing rapidly to lower energy states. The WL emission is observed to rapidly decrease, consistent with the expected carrier transfer to the QDs in the valley region. The spectrally integrated CL intensity versus time is shown in Fig. 11 with a semilogarithmic plot, from which onset rates and decay times can be extracted. The onset rate r is defined as $r = \Delta \ln(I_{CL}) / \Delta t$ and is given by the slope of the tangent to the onset curves in Fig. 11. Likewise, an exponential behavior is assumed during the decay, and decay times τ are obtained from the slopes of fitted lines as shown in Fig. 11. Onset rates of 2.9, 1.6 and 1.5 ns^{-1} were obtained for QDs on the mesa, QDs in the valley, and the WL in the valley, respectively. Decay times of 1.3, 0.92 and 0.44 ns, respectively, were also obtained, for these emissions. The larger onset rate for QDs on the mesa relative to that for QDs in the valley may be due to the ~ 100 -fold increase in the average QD density on the mesa relative to the valley region. This leads to a shorter average diffusion time of carriers before capture into the QDs when excited in close proximity to the mesa top. The difference in decay time between QDs on the mesa and in the valley may be related to differences in the electron and hole wave function overlaps between QDs in the valley and mesa regions. The reversal in the polarization anisotropy between QDs in

the valley and mesa region, as discussed in Sec. III B, also provides evidence for attendant differences in the valence-band wave functions, which ought to influence the magnitude of the oscillator strengths and electron–hole radiative lifetimes.

IV. SUMMARY AND CONCLUSIONS

We have examined the optical properties of self-assembled InAs QDs grown on prepatterned GaAs(001) substrates with polarization sensitive and time-resolved CL imaging and spectroscopy techniques. The InAs QDs were formed using a novel application in self-assembled molecular beam epitaxial growth which entailed the growth of InAs on preformed [110]-oriented stripe mesas. Interfacial In adatom migration occurred along the stripe sidewalls during growth, enabling the selective formation of linear arrays of InAs QDs on the stripe mesas. The total InAs deposition needed to induce the 2D to 3D morphology change on the stripes is less than that required to initiate QD formation on the unpatterned substrates. The QDs formed on the mesa top were found with a luminescence distribution redshifted relative to QDs in the valley region, indicating that QDs with a larger average size were formed on the mesa top. The lower density of QDs in the valley region led to a weaker emission and sharper δ -like transitions at lower beam currents, relative to emission from QDs on the mesa. CL imaging was employed to study the spatial distribution of luminescence and identified the presence of relatively small QDs situated near the edges of the valley region along the lower surface of the stripe edges. An excitation- and energy-dependent polarization anisotropy relative to the $\langle 110 \rangle$ directions was observed in CL emission. The presence of a strain may effect the relative admixtures of hh and lh characters in the valence-band wave functions, thereby inducing these polarization effects in the excitonic luminescence. A polarization anisotropy reversal was found between CL from QDs on the mesa and in the valley regions, revealing the importance of the stress anisotropy in both the formation of QDs and their subsequent optical properties. The CL was examined as a function of temperature to evaluate thermal re-emission of carriers and the associated activation energies. The carrier relaxation and recombination were further studied with time-resolved CL to measure differences in the CL onset and decay rates for QDs in the valley and mesa regions. These results should provide a basis for further experimental and detailed theoretical studies into the optical and electronic properties of self-assembled QDs grown using size-reducing and selective epitaxial growth approaches.

ACKNOWLEDGMENTS

This work was supported by the Army Research Office, Office of Naval Research, Air Force Office of Scientific Re-

search, and the National Science Foundation (RIA-ECS). The authors wish to thank Dr. R. Heitz for fruitful discussions.

- ¹N. N. Ledentsov *et al.*, *Solid-State Electron.* **40**, 785 (1996).
- ²Q. Xie, A. Kalburge, P. Chen, and A. Madhukar, *IEEE Photonics Technol. Lett.* **8**, 965 (1996).
- ³K. W. Berryman, S. A. Lyon, and M. Segev, *Appl. Phys. Lett.* **70**, 1861 (1997).
- ⁴S. Sauvage, P. Boucaud, F. H. Julien, J.-M. Gerard, V. Thierry-Mieg, *Appl. Phys. Lett.* **71**, 2785 (1997).
- ⁵N. Horiguchi, T. Futatsugi, Y. Nakata, and N. Yokoyama, *Appl. Phys. Lett.* **70**, 2294 (1997).
- ⁶R. J. Warburton, C. S. Durr, K. Karrai, J. P. Kotthaus, G. Medeirosribeiro, and P. M. Petroff, *Phys. Rev. Lett.* **79**, 5282 (1997).
- ⁷S. Guha, A. Madhukar, and K. C. Rajkumar, *Appl. Phys. Lett.* **57**, 2110 (1990).
- ⁸S. Fafard, D. Leonard, J. L. Merz, P. M. Petroff, *Appl. Phys. Lett.* **65**, 1388 (1994).
- ⁹J. -Y. Marzin, J. -M. Gerard, A. Izrael, and D. Barrier, *Phys. Rev. Lett.* **73**, 716 (1994).
- ¹⁰M. Grundmann *et al.*, *Phys. Rev. Lett.* **74**, 4043 (1995).
- ¹¹Q. Xie, N. P. Kobayashi, T. R. Ramachandran, A. Kalburge, P. Chen, and A. Madhukar, *J. Vac. Sci. Technol. B* **14**, 2203 (1996).
- ¹²A. Madhukar, Q. Xie, P. Chen, and A. Konkar, *Appl. Phys. Lett.* **64**, 2727 (1994).
- ¹³N.P. Kobayashi, T.R. Ramachandran, P. Chen, and A. Madhukar, *Appl. Phys. Lett.* **68**, 3299 (1996).
- ¹⁴Q. Xie, A. Madhukar, P. Chen, and N.P. Kobayashi, *Phys. Rev. Lett.* **75**, 2542 (1995).
- ¹⁵A. Konkar, A. Madhukar, and P. Chen, *Appl. Phys. Lett.* **72**, 220 (1998).
- ¹⁶M. Grundmann, N. N. Ledentsov, O. Stier, J. Bohrer, D. Bimberg, V. M. Ustinov, P. S. Kop'ev, and Z. I. Alferov, *Phys. Rev. B* **53**, R10509 (1996); M. Grundmann, N. N. Ledentsov, O. Stier, D. Bimberg, V. M. Ustinov, P. S. Kop'ev, and Zh. I. Alferov, *Appl. Phys. Lett.* **68**, 979 (1996).
- ¹⁷L. Brusaferrri, S. Sanguinetti, E. Grilli, M. Guzzi, A. Bignazzi, F. Bogani, L. Carraresi, M. Colocci, A. Bosacchi, P. Frigeri, and S. Franchi, *Appl. Phys. Lett.* **69**, 3354 (1996).
- ¹⁸H. Lee, W. Yang, and P. C. Sercel, *Phys. Rev. B* **55**, 9757 (1997).
- ¹⁹Y. Nabetani, T. Ishikawa, S. Noda, and A. Sasaki, *J. Appl. Phys.* **76**, 347 (1994).
- ²⁰H. Saito, K. Nishi, S. Sugou, and Y. Sugimoto, *Appl. Phys. Lett.* **71**, 590 (1997).
- ²¹F. Adler, M. Geiger, A. Bauknecht, F. Scholz, H. Schweizer, M. H. Pilkuhn, B. Ohnesorge, and A. Forchel, *J. Appl. Phys.* **80**, 4019 (1996).
- ²²W. Yang, R. R. Lowe-Webb, H. Lee, and P. C. Sercel, *Phys. Rev. B* **56**, 13314 (1997).
- ²³R. Heitz, A. Kalburge, Q. Xie, M. Grundmann, P. Chen, A. Hoffmann, A. Madhukar, and D. Bimberg, *Phys. Rev. B* **57**, 9050 (1998).
- ²⁴A. Konkar, K.C. Rajkumar, Q. Xie, P. Chen, A. Madhukar, H. T. Lin, and D. H. Rich, *J. Cryst. Growth* **150**, 311 (1995).
- ²⁵H. T. Lin, D. H. Rich, A. Konkar, P. Chen, and A. Madhukar, *J. Appl. Phys.* **81**, 3186 (1997).
- ²⁶D. H. Rich, A. Ksendzov, R. W. Terhune, F. J. Grunthaner, B. A. Wilson, H. Shen, M. Dutta, S. M. Vernon, and T. M. Dixon, *Phys. Rev. B* **43**, 6836 (1991).
- ²⁷D. H. Rich, K. C. Rajkumar, L. Chen, A. Madhukar, and F. Grunthaner, *Appl. Phys. Lett.* **61**, 222 (1992).
- ²⁸D. H. Rich, Y. Tang, and H. T. Lin, *J. Appl. Phys.* **81**, 6837 (1997).
- ²⁹Y. P. Varshni, *Physica (Amsterdam)* **34**, 149 (1967); InAs parameters were obtained from Landolt-Bornstein, in *Numerical Data and Functional Relationships in Science and Technology*, New Series, III/17a, edited by O. Madelung (Springer, Berlin, 1982), p. 297.